

ADA 081 912

9 Technical Report No. 79-04

12

to the

Office of Naval Research

Contract No. N00014-75-C-0419

15

LEVEL 4

6

MAGNETOMECHANICAL ACOUSTIC EMISSION FOR RESIDUAL STRESS AND PRIOR STRAIN DETERMINATION.

DTIC SELECTE

MAR 12 1980

10

Kanji Ono and M. Shibata
MATERIALS DEPARTMENT
School of Engineering and Applied Science
University of California
Los Angeles, California 90024

30 36

34 TR 79-04

11

October 1979

This document has been approved for public release and sale; its distribution is unlimited.

DDC FILE COPY

Reproduction whole or in part is permitted for any purpose of the United States Government.

406237

80 3 10 153

REPORT DOCUMENTATION PAGE		READ INSTRUCTIONS BEFORE COMPLETING FORM
1. REPORT NUMBER ONR Technical Report No. 79-04	2. GOVT ACCESSION NO.	3. RECIPIENT'S CATALOG NUMBER
4. TITLE (and Subtitle) Magnetomechanical Acoustic Emission for Residual Stress and Prior Strain Determination		5. TYPE OF REPORT & PERIOD COVERED Technical
		6. PERFORMING ORG. REPORT NUMBER
7. AUTHOR(s) Kanji Ono and M. Shibata		8. CONTRACT OR GRANT NUMBER (if any) N00014-75-C-0419
9. PERFORMING ORGANIZATION NAME AND ADDRESS Materials Department, 6531-Boelter Hall University of California, Los Angeles, CA 90024		10. PROGRAM ELEMENT PROJECT, TASK AREA & WORK UNIT NUMBERS
11. CONTROLLING OFFICE NAME AND ADDRESS Physics Program ONR-800 North Quincy Street Arlington, Virginia 22217		12. REPORT DATE October 1979
		13. NUMBER OF PAGES 34
14. MONITORING AGENCY NAME & ADDRESS (if different from Controlling Office)		15. SECURITY CLASS (of this report) Unclassified
		15a. DECLASSIFICATION/DOWNGRADING SCHEDULE
16. DISTRIBUTION STATEMENT (of this Report) Unlimited		
17. DISTRIBUTION STATEMENT (of the abstract entered in Block 20, if different from Report)		
18. SUPPLEMENTARY NOTES Presented at the International Conference on Acoustic Emission, 10-13 September 1979, Anaheim, California and to be published in Proceedings volume by the American Society of Nondestructive Test		
19. KEY WORDS (Continue on reverse side if necessary and identify by block number) Acoustic Emission Magnetomechanical Effect IRON, Steel, Nickel Residual Stress Heat Treatment Prior Plastic Strain Chemical Composition		
20. ABSTRACT (Continue on reverse side if necessary and identify by block number) See next page		

MAGNETOMECHANICAL ACOUSTIC EMISSION FOR RESIDUAL
STRESS AND PRIOR STRAIN DETERMINATION*

Kanji Ono and M. Shibata
Materials Department
School of Engineering and Applied Science
University of California
Los Angeles, California 90024

ABSTRACT

↙ This study evaluated magnetomechanical acoustic emission (MAE) in iron, nickel, steels and an iron-nickel alloy. The intensity of MAE increased with an increasing level of magnetization at 60 Hz and was also dependent on chemical composition, microstructure, applied stress, and prior cold work. Nickel was the highest emitter and the iron-31% nickel alloy was the lowest. Martensitic transformation and cold-working reduced MAE. Applied stress also suppressed MAE, although some enhancements were observed in nickel and A533B steel.

A model based on displacement step generation is proposed. The displacement is a consequence of domain boundary motion that alters magnetostrictive strain. The model satisfactorily explains a variety of experimental observations at least qualitatively. However, independent experiments will be needed to confirm some of the assumptions.

Results presented amply demonstrate that MAE provides the basis for a new class of nondestructive testing of residual stress and other material parameters of practical interest.

*Supported by ONR Physics Program

Accession For	Microfilm	□
MM	□	□
DDC TAB		
Unrec'd		
Serials Section		
By		
Disc. Number		
Author	Hy. G. G. des	
Article #/OR		
Dist	Special	

1. INTRODUCTION

The motion of magnetic domain walls in ferromagnetic materials produces acoustic emission (AE). This type of AE was detected during magnetization of nickel⁽¹⁾ and during elastic loading of iron.⁽²⁾ Recently, Kusanagi, et al.⁽³⁾ found applied stress dependent AE from ferromagnetic materials under alternating magnetic fields. This AE phenomenon has a potential of performing nondestructive measurements of residual stresses in structures, components and weldments.

For nondestructive measurement of residual stress, several techniques have been developed, and used for industrial applications. X-ray diffraction is the most commonly utilized.⁽⁴⁾ Techniques based on shear wave acoustic birefringence⁽⁵⁾ and magnetic Barkhausen effect⁽⁶⁾ are also developed. However, these methods are generally quite complicated and often can measure the stress only at the extreme surface layer. It appears that the newly found AE phenomenon can greatly extend the capabilities of nondestructive stress determination.

The origin of AE observed in ferromagnetic materials under alternating magnetic fields is apparently related to magnetostriction. For this reason, we call it magnetomechanical acoustic emission, to be abbreviated hereafter as MAE. In order to clarify the nature of MAE and to explore its potential for nondestructive testing applications, we examined systematically effects of applied stress and magnetic field strength in ferritic steels.⁽⁷⁻⁹⁾ Several carbon steels, A533B steel and a commercially pure iron were tested in annealed or normalized condition.

It was found that 1020 steel shows the highest AE response among the materials tested. By employing two or more AE transducers of different resonant frequencies, rms voltages were measured at different frequency ranges. Residual stress levels can be determined by monitoring the ratio of the outputs of two AE transducers for a given material condition. The amount of prior cold work can also be obtained by monitoring this AE phenomenon.

In this paper, we report the results of our recent studies on MAE as a function of chemical composition, applied stress, prior plastic deformation and microstructural variation. It is revealed that these variables produce significant changes in MAE behavior of materials and that several interesting and promising approaches to nondestructive evaluation can be developed.

2. EXPERIMENTAL PROCEDURE

Table I lists the materials and their heat treatments used in this study. Sample shape was the half-size round tensile specimen geometry per ASTM standard (E-8) with the 6.3 mm diameter and 32 mm length reduced section. The total length of the sample was 84 mm and the threaded grip section was 12.7 mm diameter except for magnetic iron and 1020 steel, which had 16 mm diameter thread. Samples were heat treated after machining. One exception to this sample geometry was Fe-Ni alloy, for which a sheet of 0.6 mm x 10 mm x 100 mm was used. Experimental set-up for MAE testing is schematically shown

TABLE I
Materials and Heat Treatment

<u>MATERIALS</u>	<u>HEAT TREATMENT</u>
Iron (Ferrovac E)	1183 K 1 hr, FC
Iron (Magnet)	1183 K 1 hr, FC
AISI 1020	1183 K 1 hr, FC
AISI 1045	1123 K 1 hr, AC
AISI 1065	1123 K 1 hr, AC
AISI 1074	1173 K 1 hr, FC
	1173 K 1 hr, O-Q plus 773 or 923 K 1 hr, AC
ASTM A533B Cl .2	As Received
Nickel (Ni-200)	1183 K 1 hr, FC
Fe-31%Ni	1125 K WQ

in Fig. 1. Transducers for AE detection were attached to the flat ends of a sample. Coupling utilized viscous resin, wax or cyanoacrylate glue. Resonant transducers with six different center frequencies were used in the study. These were manufactured by AET, Sacramento, CA. and designated as Models AC30, AC175L, MAC300, MAC500, AC750, and AC1500L. The model number represents the nominal center frequency. The transducer output was amplified 60 dB using Model 160 preamplifier of AET and its rms voltage was determined by Model 3400A rms voltmeter of Hewlett-Packard. A suitable bandpass filter was also used.

Magnetic field was generated by an encircling coil, powered by 60 Hz commercial source. Maximum applied voltage was 140 V, which generated the field of 26 kA/m rms at the center of the solenoid*. When a sample is inserted, this field changes due to eddy current generation and changes in the inductance of the solenoid. In this report, we use the magnetic field readings for an empty coil, which are called "applied magnetic field strength", H. The magnetic field strength in a sample was also measured using a Hall probe (Sprague UGN 3501 T). The probe was attached to an end of the sample (in place of one of AE transducers). While this reading is not identical to the magnetic field level of the gauge section of the sample, relative changes can be indicated. This Hall probe output is termed "magnetic field strength", H_s .

*In our previous reports, the field level was reported at one-tenth of the actual value due to an error in converting Oersted to A/m.

Stressing and plastic deformation of a sample utilized a floor model Instron. MAE behavior of materials at zero stress was also tested in an all wood sample support. Results were identical to those obtained with either magnetic or nonmagnetic loading devices used with the Instron.

3. RESULTS

3-1. Material Effects

Typical results of AE output (referred to at the preamplifier input) vs. the applied field strength are shown in Fig. 2. Here, an AC175L transducer was used and external stress was not applied. The solid line in Fig. 2 is the response of a commercially pure iron (magnet iron). All materials in the figures were tested in either annealed or normalized condition except for A533B steel, which was in the as received condition. Nickel 200 shows the highest MAE response and Fe-31%Ni alloy the lowest at any applied field strength level. Direct comparison of the observed MAE levels among iron, nickel and steels can be made because of identical geometry. Nickel and iron start to exhibit MAE at the lowest level of H. As the carbon content of steel increases, a higher value of H becomes necessary for observable MAE. At the highest value of H, nickel still produced the highest MAE level, but iron produced the lowest MAE level among the round bar samples. In all cases, MAE level tended to saturate, although saturation level was not reached in any. The low MAE response of Fe-31%Ni alloy appears to be intrinsic and not due to its

sheet geometry. This is confirmed by testing iron and nickel sheets of similar dimensions. Here, a transducer was coupled to the broad face and the sample was magnetized along its longest dimension. For iron or nickel, MAE output was greater than that of a round bar tensile specimen.

The compositional effects on MAE in iron and steel are summarized in Fig. 3, where the AE intensity (with an AC175L transducer) at $H = 22.5$ kA/m is plotted against the nominal carbon content for three tensile stress levels. At zero stress, a maximum was observed at the carbon content of 0.2%. At higher stresses, the maximum AE level shifted to about 0.4% carbon.

Frequency distribution of MAE signals was examined using six different transducers. Since the sensitivities and the bandwidth of these transducers were not calibrated, the only approximate comparison between different frequency ranges can be made. Results for Ferrovac E iron, 1020 and 1074 steels are shown in Fig. 4. A peak in MAE intensity was found at 175 and 300 kHz for 1020 and 1074 steels, respectively. On the other hand, MAE level decreased with frequency in the case of iron. Since the elastic properties of these materials are similar and all the samples have the longitudinal resonance frequency below 100 kHz, the observed differences indicate the intrinsic behavior of MAE signals in these materials. While we could not obtain true frequency spectra of MAE signals, it is obvious that significant frequency contents are distributed within the range we have examined

(30 to 1500 kHz). When this frequency effect is taken into account, we find the composition effect to be also frequency dependent. For example, 1040 steel produced the maximum in MAE in a similar plot as in Fig. 3, when a transducer of 500 kHz center frequency was used.

3-2. Stress Effect

An example of variation in the AE intensity applied magnetic field strength curves due to external stress is shown in Fig. 5. Here, the results of A533B steel are given for two transducers (AC175L and MAC500) at three levels of tensile stress, 0, 172 and 344 MPa and one compressive stress of -28 MPa. Significant drop in the AE intensity was observed by applying tensile stress. On the other hand, a slight increase in MAE was found at a small compressive stress. At higher levels of compressive stress, however, the level of MAE decreased.

Effects of stress on MAE of A533B steel, nickel and iron are shown in Figs. 6, 7 and 8. Applied H level was fixed in these tests, and their values were selected so as to obtain MAE levels of about 7 μ V at zero stress. Because of the variation in permeability, however, the magnetic field of a sample was not constant. Changes in H_s are shown in these figures by broken lines. MAE in A533B steel and nickel increased slightly with the application of small compressive stress and reached a maximum at -28 and -10 MPa, respectively. In iron, MAE was highest at zero stress. In all the cases, MAE level decreased under high stress, either tension or compression. The observed stress dependencies of MAE level decreased under high stress, either tension or compression. The observed stress dependencies of MAE were dissimilar to each other and had no direct relation with changes in H_s . In A533B steel, H_s reached a maximum at 50 MPa. In nickel, an opposite trend was found.

H_s in nickel increased with the reduction of tensile stress or the increase in compressive stress. In iron, H_s had a maximum at zero stress and followed a similar trend as MAE level.

Changes in MAE level were most dependent on stress in A533B steel under tension, as shown in Fig. 6. Changes under compressive stress were generally smaller than the tension side. Again, stress dependence of MAE was a function of frequency detected and of the level of applied magnetic field, H . These aspects were reported previously.⁽⁷⁾

3-3. Microstructural Effects

When the carbon content of iron-carbon alloys is varied, relative fractions of ferrite and pearlite are changed, which in turn affect MAE behavior. This effect was described in Sec. 3-1 (see Fig. 3). When the carbon content is fixed, heat treatment alters the microstructure of a steel. Figure 9 shows the level of MAE against H of 1074 steels in the annealed, oil-quenched (O.Q) and O.Q. plus tempering conditions. When 1074 steel was quenched, MAE output was severely depressed in comparison to the annealed condition. Tempering of oil-quenched samples at 773 K restored MAE to about one-third the level of the annealed sample. Further tempering at 923°K increased the level to 70% of the annealed sample.

A similar effect of quenching was observed in A533B steel samples.⁽⁷⁾ In this steel, normalizing also reduced the MAE level significantly. Tempering at 873°K after quenching or normalizing restored MAE to the starting condition (as received; quenched and tempered in a thick plate form).

3-4. Plastic Deformation Effects

Influence of prior cold work on MAE behavior was studied using A533B and 1020 steels. The samples were progressively deformed in tension and their MAE responses were measured. Stress-strain curves are given in Fig. 10. On the curves are markers, where MAE measurements were made. An example of plastic deformation effect is shown in Fig. 12, where MAE outputs from an MAC500 transducer were plotted against stress at applied magnetic field of 22.5 kA/m. Initially, a sharp stress drop of MAE occurred as the stress level was raised to 50 MPa. This was also noted in Fig. 6. However, the initial steep stress dependence was eliminated by plastic deformation of 1.4%. When the sample was deformed 15%, the initial decrease in MAE with stress was completely gone and instead a slight increase was observed. The shape of stress dependence curves changed from concave down to concave upward with the addition of plastic strain. At zero stress, the MAE level decreased with strain, but strain dependence was more complex at higher stress levels.

4. DISCUSSION

4.1. Previous Studies on MAE

Magnetization of a ferromagnetic material is discontinuous due to the stepwise motion of magnetic domain walls.^(10,11) Such domain wall movements produce the well-known Barkhausen effect,^(12,13) which observes the changes in magnetic flux lines passing through a sensing coil. Lord⁽¹⁾ attributed MAE found in cold worked nickel rods to abrupt domain wall motion, since the steep portion of the hysteresis curve generates the maximum Barkhausen noise and observed acoustic emission.

Kusanagi et al.⁽³⁾ examined MAE from nickel and steels using alternating magnetic fields. They considered magnetic domains A and B with the direction of magnetization $(\alpha_1, \alpha_2, \alpha_3)$ and $(\beta_1, \beta_2, \beta_3)$, respectively, where α_i and β_i are direction cosines. When the domain wall moves, increasing the volume of domain A by Δv and decreasing that of domain B by the same amount, the decrease in the elastic strain energy can be calculated and expressed by^(3,10)

$$\begin{aligned} \Delta E_{el} = & \left[\frac{3}{2} \lambda_{100} \sigma \{ (\beta_1^2 - \alpha_1^2) \gamma_1^2 + (\beta_2^2 - \alpha_2^2) \gamma_2^2 + (\beta_3^2 - \alpha_3^2) \gamma_3^2 \} \right. \\ & + \frac{3}{2} \lambda_{100} (c_{11} - c_{12}) \{ (\beta_1^2 - \alpha_1^2) e_{11}^i + (\beta_2^2 - \alpha_2^2) e_{22}^i + (\beta_3^2 - \alpha_3^2) e_{33}^i \} \\ & + 3 \lambda_{111} \sigma \{ (\beta_1 \beta_2 - \alpha_1 \alpha_2) \gamma_1 \gamma_2 + (\beta_2 \beta_3 - \alpha_2 \alpha_3) \gamma_2 \gamma_3 + (\beta_3 \beta_1 - \alpha_3 \alpha_1) \gamma_3 \gamma_1 \} \\ & \left. + 3 \lambda_{111} c_{44} \{ (\beta_1 \beta_2 - \alpha_1 \alpha_2) e_{12}^i + (\beta_2 \beta_3 - \alpha_2 \alpha_3) e_{23}^i + (\beta_3 \beta_1 - \alpha_3 \alpha_1) e_{31}^i \} \right] \Delta v \quad (1) \end{aligned}$$

where $\sigma(\gamma_1, \gamma_2, \gamma_3)$ is applied or residual stress with γ as the direction cosines, λ_{100} and λ_{111} are the magnetostriction coefficients along $\langle 100 \rangle$ and $\langle 111 \rangle$, respectively, c_{11} , c_{12} and c_{44} are the elastic stiffness and e_{jk}^i is the internal strains⁽³⁾ that causes reversible magnetic domain wall movement under weak external magnetic field, respectively.

Kusanagi et al.⁽³⁾ postulated that the rms voltage of MAE, V_r , is given by

$$V_r = \frac{C}{T} \int \overline{\Delta E_{el}} n(H) dH, \quad (2)$$

where C is a constant, T is the period of external magnetic field H , $\overline{\Delta E_{el}}$ is the average of ΔE_{el} given by Eq. (1) and $n(H) dH$ is the number of sites where ΔE_{el} is released upon the change of the field from H to $H + dH$, respectively. From Eqs. (1) and (2), they arrived at the following conclusions:

1. Only the movement of 90° domain wall contributes to MAE.
2. When the direction of easiest magnetization is $\langle 100 \rangle$ (e.g. steel), only the first and second terms of Eq. (1) make contributions, whereas, in materials with $\langle 111 \rangle$ direction of easiest magnetization (e.g. nickel), only the third and fourth terms contribute to AE. For each case, λ_{100} or λ_{111} is one of the factors that determine the AE level.
3. The number of sites of elastic energy release, $n(H)$ is also one of the primary factors determining the AE intensity due to magnetization. It appears that $n(H)$ is important in consideration of stress dependency.

Since AE output is expected to reflect the release of strain energy in a material, the above postulate may have a reasonable basis. However, the strain energy postulate of Kusanagi et al.⁽³⁾ predicts no acoustic emission when a material is well annealed (no internal strain) and is not subjected to external stress. Moreover, Eq. (1) predicts increases in ΔE_{el} with external stress (σ) and with internal strain (e_{ij}^i). These predictions are contrary to experimental observations, which showed reduced MAE activities with increasing stress and with increasing cold work that results in higher internal strain. Consequently, we conclude that the linkage of ΔE_{el} and MAE is untenable and a different mechanism must be sought as the source of MAE.

4.2. A New Model of MAE

We propose that a sudden change in displacement that accompanies the motion of a magnetic domain wall generates MAE. The displacement results from differences in magnetostrictive strains in the two domains, one of which expands by ΔV^* . The magnitude and direction can be described by an inelastic strain tensor Δe_{ij}^* .

within ΔV^* . Abrupt imposition of $\Delta \epsilon_{ij}^*$ generates stress waves, which are detected elsewhere by an AE transducer as MAE.

In order to correlate $\Delta \epsilon_{ij}^*$ due to domain wall motion to the observable AE output of a transducer, we employ the theory developed by Malén and Bolin⁽¹⁴⁾ and extended recently by Ono.⁽¹⁵⁾ It uses the dynamic Green's function method and assumes a particular time-function for $\Delta \epsilon_{ij}^*$ generated in a small volume ΔV^* embedded in an infinite isotropic medium. The time dependence of $\Delta \epsilon_{ij}^*$ has sigmoidal shape following the Gauss error function. Taking the rise time τ into account, the peak output of a resonant AE transducer (V_p) is given by

$$V_p = C' \Delta \epsilon^* \Delta V^* / \tau \quad (3)$$

where C' is a constant including the elastic moduli and the distance between the source and transducer and $\Delta \epsilon^*$ is the average uniaxial strain component of $\Delta \epsilon_{ij}^*$ applicable here. Ono's extended theory further postulates that when numerous AE events excite the AE transducer at a random interval, the rms output voltage (V_r) is given by

$$V_r = C'' \sqrt{\dot{N}} V_p \quad (4)$$

where C'' is a constant and \dot{N} is the rate of AE events, respectively.

Let us now consider the parameters that affect V_r of MAE. The magnitude of $\Delta \epsilon^*$ is dictated by the magnetostriction coefficients of the domains that are separated by the moving domain boundary. It is obvious that the motion of 180° domain wall produces no displacement, but that 90° domain walls result in finite $\Delta \epsilon^*$. As $\Delta \epsilon^*$ is proportional to the magnetostriction coefficient, λ , it is expected that the intensity of MAE depends linearly with λ . (Note that the value of λ considered here for each domain corresponds not to magnetic field dependent apparent magnetostriction of polydomain materials, but to the saturation magnetostriction.) When a material is magnetized the easiest along a certain crystallographic direction (e.g. $\langle 100 \rangle$ in iron and $\langle 111 \rangle$ in nickel), the

magnetization direction of a domain initially coincides with the particular direction. At fields near saturation, the magnetization direction rotates. Again, AE is expected in proportion to λ if the rotation occurs discontinuously and heterogeneously.

The volume of each domain expansion ΔV^* is inversely proportional to the density of pinning points, such as domain boundary junctions, second phase particles, dislocations and grain boundaries. When the pinning points are encountered infrequently, ΔV^* is expected to vary with the square of the domain size of a^2 . When ΔV^* becomes smaller, the AE output decreases despite the fact the the number of sites where the domain boundary can jump increases for the same total volume. This increase of jump sites implies a higher rate of AE events (\dot{N}). According to Eq.(4), however, the effect of ΔV^* on V_r cannot be compensated by a higher \dot{N} . Both of these parameters, ΔV^* and \dot{N} , are greatly affected by the level of applied field, the difference in the magnetization directions and the strength of pinning points.

The total volume of magnetization under alternating fields depends on the skin depth due to eddy current effect. It is inversely proportional to the square-root of the product of the frequency of the field, the conductivity and permeability of a ferromagnetic material. Since the permeability depends strongly on the level of magnetization, ^(10,16) the depth of penetration varies also. Effects of demagnetization ⁽¹⁷⁾ due to sample geometry reduce the effective field strength within a sample in comparison to the field applied. When samples of different shapes are employed, demagnetization factors produce different levels of magnetization in the samples. Since the demagnetization effect is dependent on the level of magnetization, the permeability also affects the field strength within the samples of an identical geometry.

Abruptness of domain boundary motion is reflected in the rise time (τ) of a

stepwise increase in $\Delta\epsilon^*$. Even when $\Delta\epsilon^*$ and ΔV^* remain unchanged, AE intensities depend strongly on τ according to Eq. (3). It is expected that τ varies with the mobility (or conversely, viscous damping factor) of domain boundary, the degree of pinning, the driving force for domain boundary motion and the rate of change in applied magnetic field.⁽¹⁸⁾ The higher is the domain boundary mobility, the driving force or the rate of field change, the smaller becomes τ . A higher driving force for domain boundary motion should aid in reducing τ , as a higher speed of boundary motion can be attained more readily. Viscous damping factor has an opposite effect. Whereas weak pinning of a domain boundary may allow its quick release from the pinning point, strong pinning is expanded to the critical geometry. Thus, effect of pinning on τ cannot be predicted unequivocally. It appears that unstable expansion of domain boundary should effectively reduce τ at a strong pinning point.

Let us summarize the salient features of the model for MAE proposed here. MAE arises from numerous displacement steps having short rise times due to the differential magnetostrictive strain produced by abrupt magnetic domain boundary movements. Noting random arrivals of AE pulses, the rms voltage of MAE is given by

$$V_r = C''' \sqrt{\dot{N}} \Delta\epsilon^* \Delta V^* / \tau \quad (5)$$

In order to assure nonzero $\Delta\epsilon^*$, λ must be finite and the domain wall in motion must not be of 180° type. (In this respect, MAE distinguishes itself from Barkhausen effect.) Domain size and/or the density of pinning points dictates \dot{N} and ΔV^* , but the latter has a greater influence on V_r . Factors determining the dynamical behavior of domain wall motion affect V_r mainly through their effects on τ . Although details of MAE behavior can hardly be predicted by the present model, we can construct consistent qualitative arguments for various observations concerning MAE. These will be given next.

4.3. Discussion of Observed MAE Characteristics

Materials with different values of λ are first considered. Experimental findings presented in 3.1. indicated that nickel and Fe-31% Ni alloy were the two extremes in MAE outputs. It is known that the Fe-Ni alloy has nearly zero magnetostriction.⁽¹⁰⁾ Thus, the near absence of MAE in this material agrees with Eq. (5). On the other hand, nickel has the largest λ among the materials tested. Again, this is readily explained through Eq. (5).

In steels of varying composition, the MAE level increased initially, then declined with the carbon content. Microstructure of these steels consisted of ferrite and pearlite. An individual domain of ferrite is expected to have similar magnetostriction as pure iron.⁽¹⁰⁾ Consequently, the observed compositional effects must be explained via changes in the pinning point density, ΔV^* and τ . With more carbide particles or lamellae in steels compared with pure iron, observed increase in MAE appears to originate from the reduction in τ . Domain walls in pure iron probably are compliant to changing magnetic field, producing less jerky motions. As the carbon content exceeds 0.4%, more than a half of steel becomes pearlite. MAE behavior is thus controlled mainly by pearlite. Because of fine lamellar structures, ΔV^* is small and is expected to reduce the AE level.

Observed frequency distributions of MAE indicate the shift of the peak intensity range to higher frequencies. Presently, it is not certain whether the shift is related to τ , but the trend appears to be as may be expected: i.e. more high frequency content for shorter τ .

In pure iron and nickel, AE starts to be observed at the lowest H level. Since the domain sizes are expected to be the largest due to a small density of pinning points, the required levels of applied field are also low. This is because the required field for critically bowing out the domain boundary is in-

versely proportional to the domain size.

Consider the stress effect on MAE next. Regardless of materials, high stress in tension or compression reduced MAE from the zero stress level. Depending on the material, the magnetic field strength within a sample (H_s) varies with stress (of Fig. 6-8). Such stress dependence undoubtedly explains a portion of the observed effect on the MAE level. Remaining portion appears to arise from the reduction in the size of magnetic domains with stress. Dijkstra⁽¹⁹⁾ and Martin observed that the domain size decreased in proportion to the inverse square root of applied stress. The reduction is in part due to internal stress around inhomogeneities such as pearlite, carbide particles and non-metallic inclusions.⁽²⁰⁾ Nonuniform stress fields contribute to magnetic anisotropy.⁽¹¹⁾ When the domain size becomes smaller under stress, V_r is affected through ΔV^* term in Eq. (5). It is likely that τ and \dot{N} are also affected.

In some materials, MAE showed a peak at a nonzero stress. A533B steel (Fig.6) and nickel (Fig. 7) exhibited a maximum in V_r at slightly compressive stresses. Kusunagi et al.⁽³⁾ reported similar maxima in a mild steel and in nickel. The maximum found in the mild steel sample was similar to our findings. However, the nickel sample had two peaks, one in tension and the other less prominent one, in compression. The different behaviors of nickel in these two studies may be due to the geometry of samples and require further investigation for their clarification. If steels with positive magnetostriction have a peak under tensile stress and nickel with negative λ has a peak under compressive stress, and explanation could be sought through the magnetoelastic interaction.⁽¹⁶⁾ The interaction energy can be obtained by either the first or third term of Eq. (1). In steels magnetization lengthens the sample in the tensile direction. This should provide a higher driving force for a more complete alignment of the spins. The same can be true for nickel under compressive stress. The higher

the driving force (equivalent to a higher magnetic field strength), the larger should MAE outputs become. Thus, only our observations concerning nickel (a peak under compressive stress) fit the expected behavior. It should be noted that the magnetoelastic interaction predicts higher H_s values in steel under tension and in nickel under compression. Our observations in A533B steel and nickel agree with the prediction (ct. Figs. 6 and 7).

MAE characteristics of steel samples with various microstructures can also be understood using our model. When a steel is quenched and has a martensitic structure, it has a high concentration of dissolved interstitial carbon atoms and a very high density of dislocations and boundaries of martensite plates (or laths). The defect structure severely limits the mobility of domain boundaries and refines the domain structures. These conditions lead to low MAE outputs as observed in this study (ct. Fig. 9). As tempering removes the interstitial carbon from the matrix (into carbide particles) and dislocations by recovery and recrystallization, MAE activities are expected to increase. The observations on 1074 steels confirmed this behavior. Essentially all the excess carbon atoms are expected to precipitate out as carbide after O.Q. plus tempering at 773 K. In this condition, the reduction of MAE level in comparison to the annealed state can thus be attributed to fine carbide particles and dislocation substructures, which reduce ΔV^* by domain refinement and increase τ by limiting the mobility of domain boundaries. After tempering at 923 K, a distribution of small carbide particles is expected in the recrystallized matrix. The observed MAE level was still lower than that of the annealed sample. This is apparently due to carbide particles, distributed uniformly.

After severe plastic deformation, MAE levels generally decreased from that of an annealed sample of the same material. However, some materials exhibited a higher MAE intensity after a small amount of deformation. The decrease in MAE

apparently results from the reduction in domain size and in the mobility of domain boundary. Nonuniform internal stresses and a high density of dislocations contribute to such changes. The observed increase in MAE (found in pure iron, 1020 steel and nickel) can be interpreted as due to the reduction in τ provided by the presence of a low density of pinning points. This behavior may be likened to the observed increase in MAE by adding 0.2% carbon to pure iron. By introducing a small number of pearlite, MAE of 1020 steel became higher than that of pure iron.

When additional parameters, the stress dependence and the frequency range of AE measurements, are included in the consideration, complex effects of plastic deformation become impossible to analyze. Yet, significant changes were observed, awaiting future investigation.

5. CONCLUSION

1. Magnetomechanical acoustic emission (MAE) was observed in iron, nickel, steels and an iron-nickel alloy. The intensity of MAE was dependent on the chemical composition of material, microstructure, applied stress, and prior cold work.
2. MAE level increased with increasing magnetic field strength that varied at 60 Hz. Nickel produced the highest level of MAE, whereas iron-31% Ni alloy and quenched 1074 steel produced very low levels of MAE.
3. At a given field strength, tensile on compressive stress generally reduced the MAE output, although a maximum was observed in A533B steel and nickel under compressive stress.
4. Increase in the number of inhomogeneities and obstacles for domain movement reduced the intensity of MAE with some exceptions.
5. A new model is proposed to explain various characteristics of MAE. It is based on the generation of a displacement step with a short rise time (τ), which results from an abrupt expansion of a magnetic domain boundary (ΔV^*) imposing a differential magnetostrictive strain ($\Delta \epsilon^*$).
6. The model predicts the rms voltage of continuous type MAE (V_r) as

$$V_r = (\text{constant}) \sqrt{\dot{N}} \Delta \epsilon^* \Delta V^* / \tau ,$$
 where \dot{N} is the rate of AE events.
7. Most of experimental observations on MAE can be explained qualitatively by the model with the aid of previous knowledge on the behavior of ferromagnetic materials.

Acknowledgement

The authors are grateful for financial support by the Physics Program, the Office of Naval Research.

REFERENCES

1. A.E. Lord, Jr., "Physical Acoustics", Vol., XI, edited by W.P. Mason and R.N. Thurston, Academic Press, New York, 1975 p. 290.
2. F.P. Higgins and S.H. Carpenter, Acta Met. 26, (1978) 133.
3. H. Kusanagi, H. Kimura and H. Sasaki, "Proc. 1st General AE Symposium" hold in Tokyo, Japan, Dec. 1977, Japan Nondest. Insp., Tokyo, 1977 p. 145; see also J. Appl. Phys. 50 (1979) 2985.
4. B.D. Cullity, "Elements of X-ray Diffraction", 2nc edition, Addison-Wesley, Reading, Massachusetts, 1978 pp. 447-478.
5. W.N. Clotfelter and E.R. Risch, NASA TM X-73315, June 1976.
6. C.G. Gardner, G.A. Matzkanin and D.L. Davidson, Inst. J. Nondest. Test. 3 (1971) 131.
7. K. Ono and M. Shibata, "Magnetomechanical Acoustic Emission of Iron and Steel", ONR Tech. Report 79-01, University of California, Los Angeles, January 1979.
8. M. Shibata and K. Ono, "Acoustic Emission Method for Stress and Strain Determination" Proceedings of the Institute of Acoustic Conference, April 1979, Chelsea College, London, England.
9. K. Ono and M. Shibata, "Magnetomechanical Acoustic Emission for Residual Stress Measurements in Railroad Rails and Wheels", Proceedings of Conference on NDT for Measuring the Longitudinal Force in Rails, Fed. Railway Adm. and Am. Assoc. of Railroads, Feb. 1979, Washington, D.C.
10. R.M. Bozorth, "Ferromagnetism", van Nostrand, New York, 1951.
11. S. Chikazumi, "Physics of Magnetism", Wiley, New York, 1964.
12. H. Barkhausen, A., Physik, 20, (1919) 401.
13. K. Stierstadt, "Der Magnetische Barkhausen-Effekt, Springer Tracts in Modern Physics", Vol. 40, Springer-Verlag, Berlin, 1966, pp. 2-106.

14. K. Malén and L. Bolin, Phys. Stat. Sol. (b) 61 (1974) 637.
15. K. Ono, "Acoustic Emission Arising from Plastic Deformation and Fracture", Fourth AE Symposium, Sept. 1978; Fundamentals of AE, Proc. of AE Session, ASA-ASJ meeting, Honolulu, Hawaii, Dec. 1978, (in press).
16. B.D. Cullity, "Introduction to Magnetic Materials", Addison-Wesley, Reading, Massachusetts 1972, pp. 248-286.
17. J.L. Snoek, "New DevelopMents in Ferromagnetic Materials", Elsevier, New York, 1949.
18. C. Kittel and J.K. Galt, Solid State Phys., 3 (1956) 437.
19. L.J. Dijkstra and U.M. Martins, Rev. Modern Phys., 25 (1951) 146.
20. M. Shibata and K. Ono, Acta Met., 26 (1978) 921.

FIGURE CAPTION

1. Schematic diagram of experimental setup.
2. Acoustic emission vs. applied magnetic field strength for seven materials at 175 kHz without applied stress.
3. Acoustic emission at three stress levels (0,69 and 138 MPa) vs. carbon content in iron and plain carbon steels.
4. Acoustic emission vs. the center frequency of six transducers for Ferrovac E iron, 1020 steel and 1074 steel.
5. Acoustic emission vs. applied magnetic field strength for A533B steel at three tensile stress levels (0,172 and 344 MPa) and one compressive stress level (-28 MPa). Solid lines are for 500 kHz and dotted lines for 175 kHz.
6. Acoustic emission and magnetic field strength (H_s) vs. applied stress for nickel 200 at $H = 5$ kA/m.
7. Acoustic emission and magnetic field strength (H_s) vs. applied stress for A533B steel at $H = 14$ kA/m.
8. Acoustic emission and magnetic field strength (H_s) vs. applied stress for Ferrovac E iron at $H = 20$ kA/m.
9. Acoustic emission vs. applied magnetic field strength at 175 kHz without applied stress for 1074 steel with different heat treatments.
10. Stress-strain curves of 1020 and A533B steels. Circles indicate the strain levels where MAE measurements were made.
11. Background corrected AE level (500 kHz) vs. applied stress for A533B steel, deformed 0, 1.4 and 15%. Applied magnetic field strength was 22.5 kA/m.

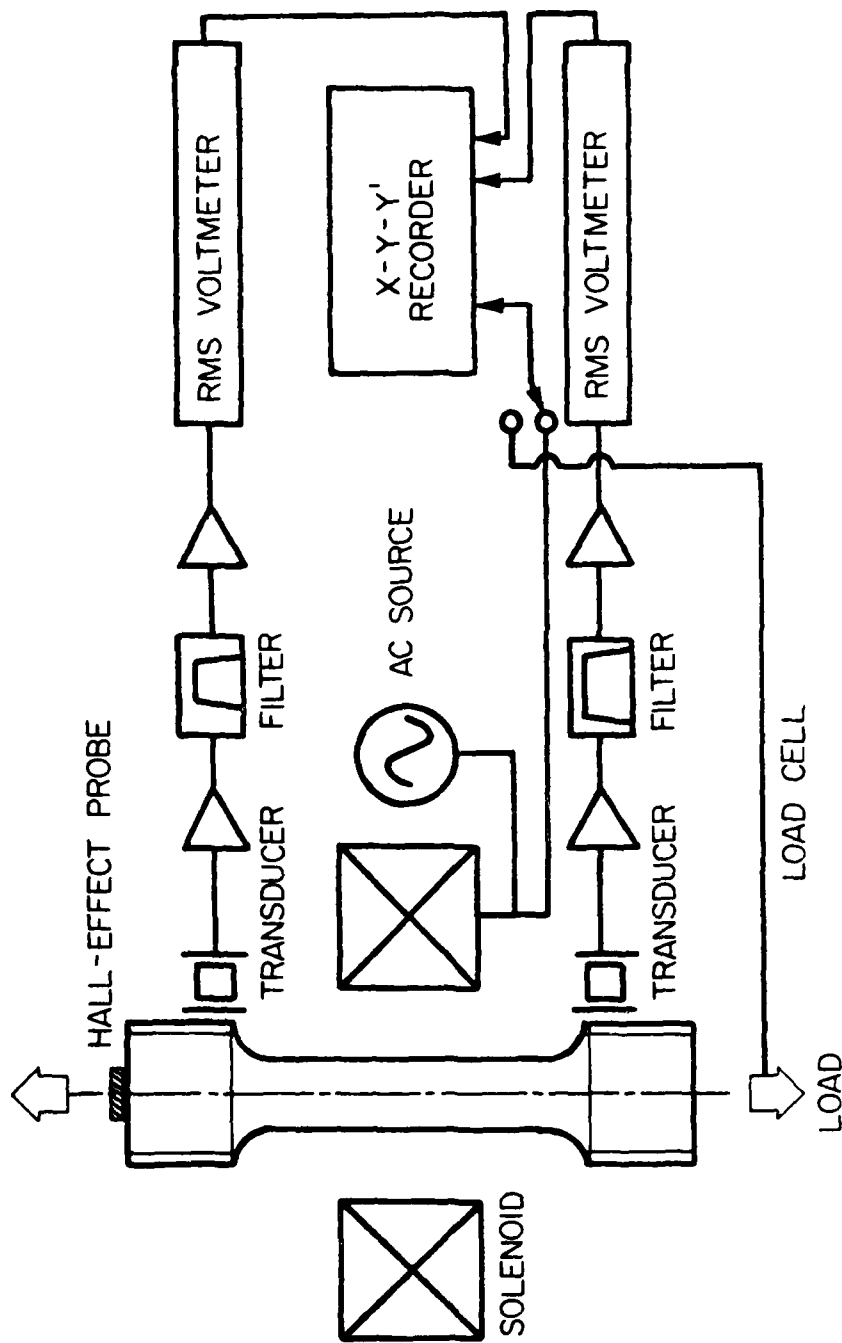


Figure 1. Schematic diagram of experimental setup.

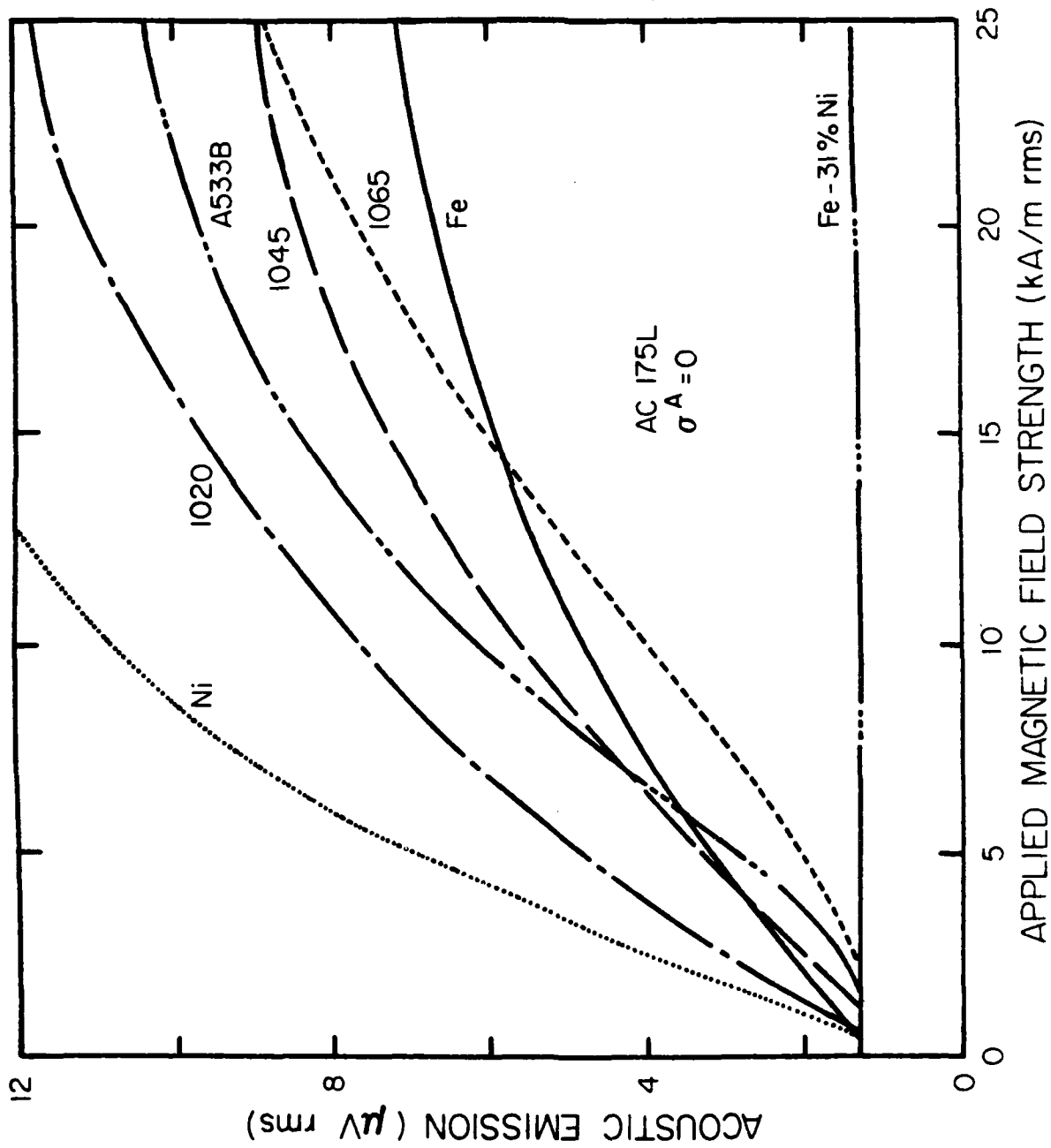


Figure 2. Acoustic emission vs. applied magnetic field strength for seven materials at 175 kHz without applied stress.

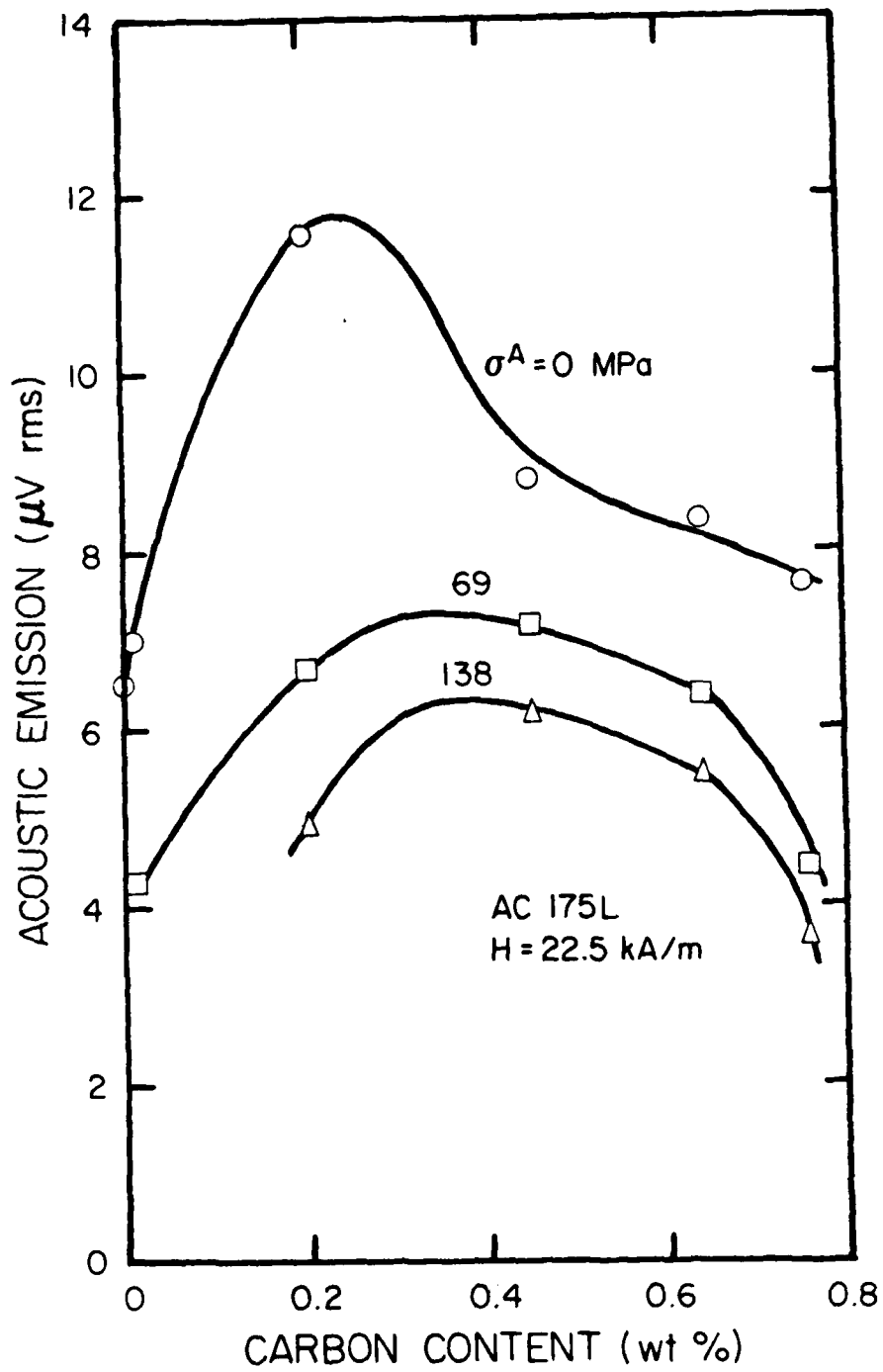


Figure 3. Acoustic emission at three stress levels (0, 69 and 138 MPa) vs. carbon content in iron and plain carbon steels.

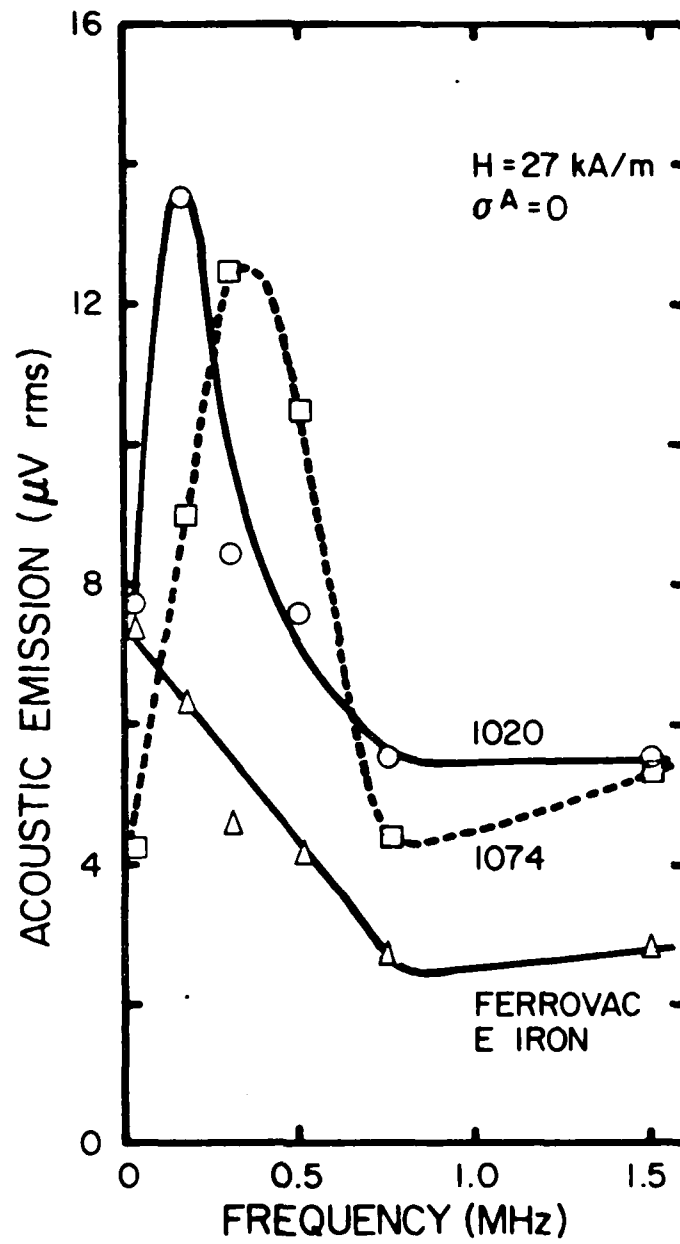


Figure 4. Acoustic emission vs. the center frequency of six transducers for Ferrovac E iron, 1020 steel and 1074 steel.

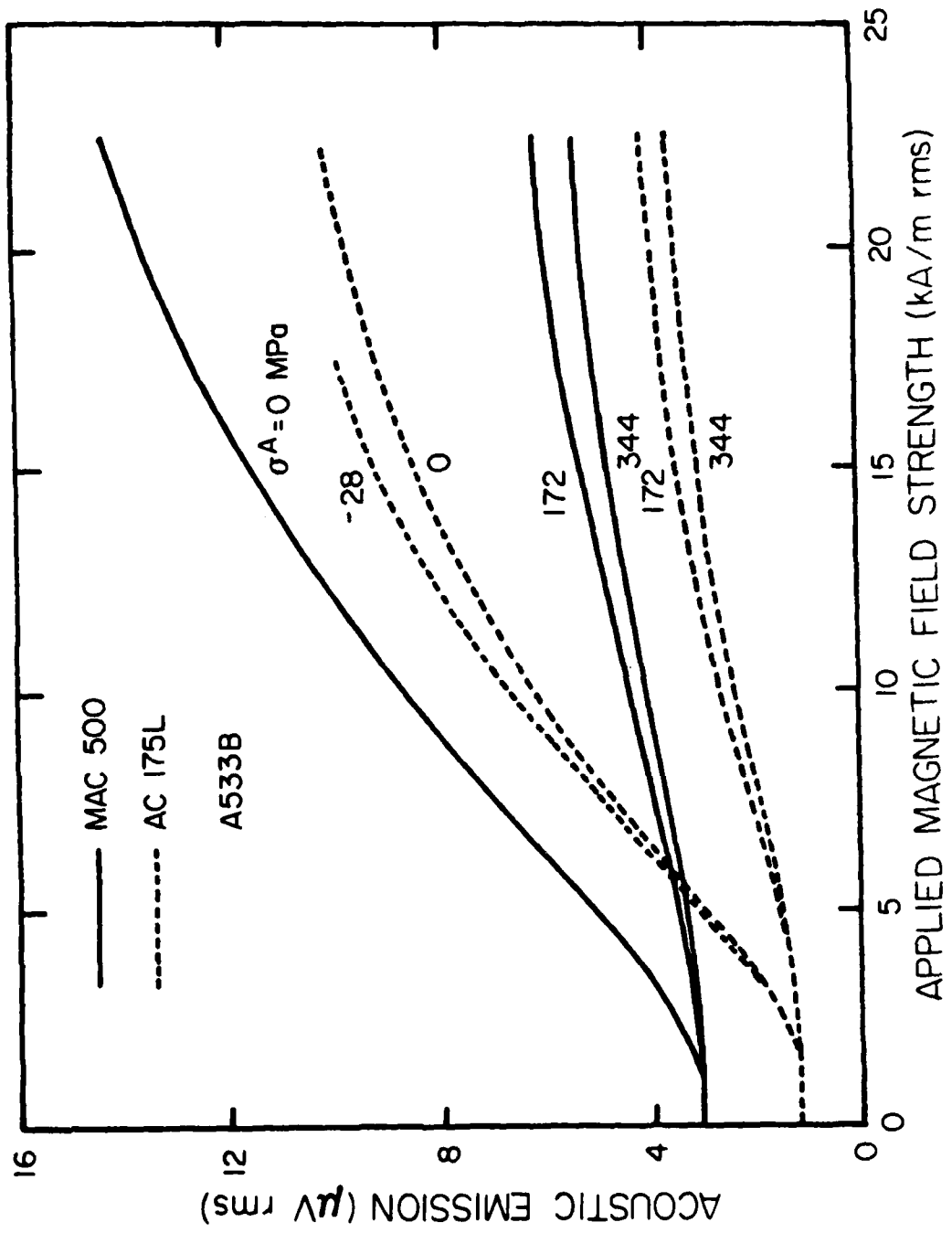


Figure 5. Acoustic emission vs. applied magnetic field strength for A533B steel at three tensile stress levels (0, 172 and 344 MPa) and one compressive stress level (-28 MPa). Solid lines are for 500 kHz and dotted lines for 175 kHz.

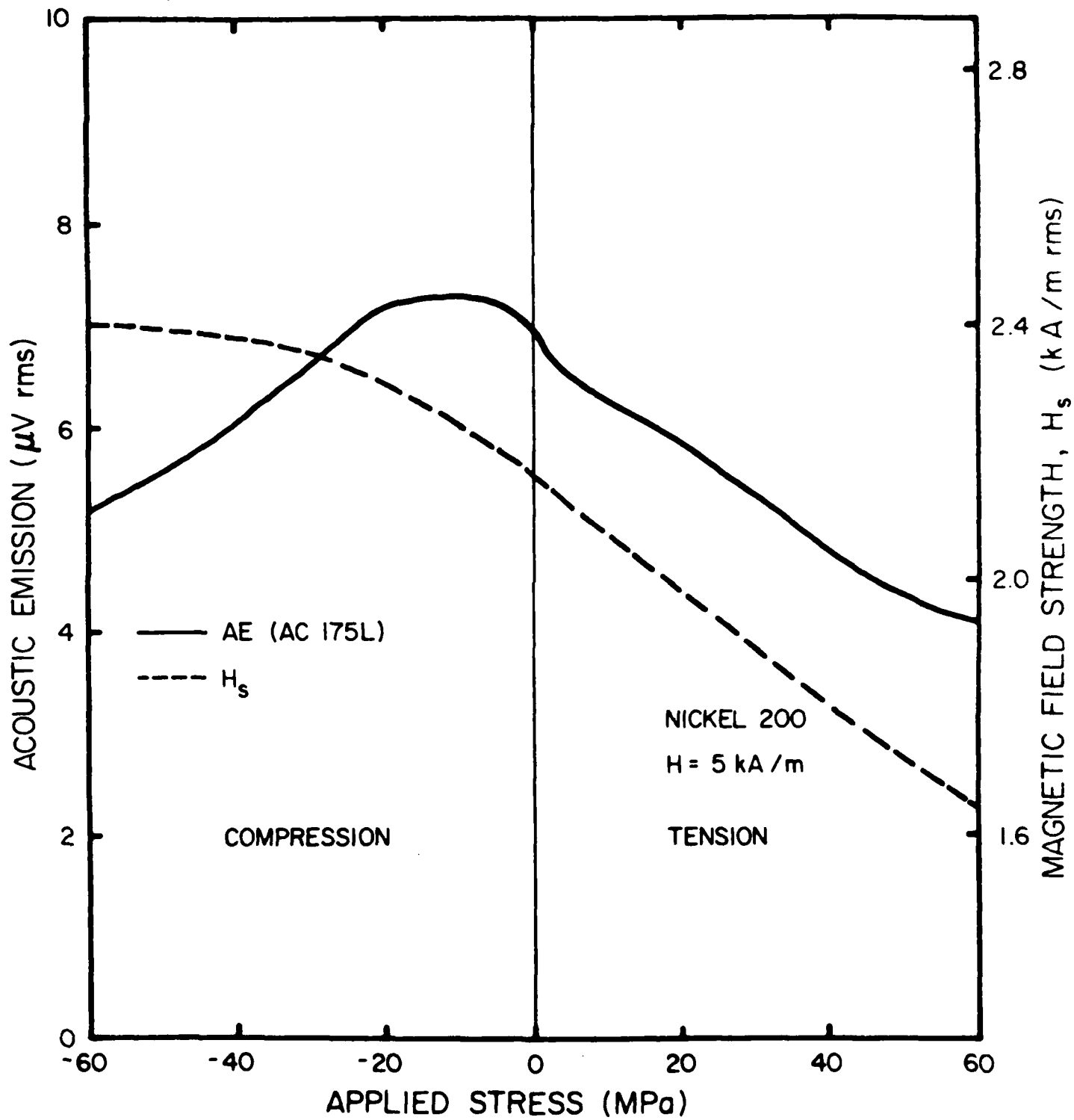


Figure 6. Acoustic emission and magnetic field strength (H_s) vs. applied stress for nickel 200 at $H = 5 \text{ kA/m}$.

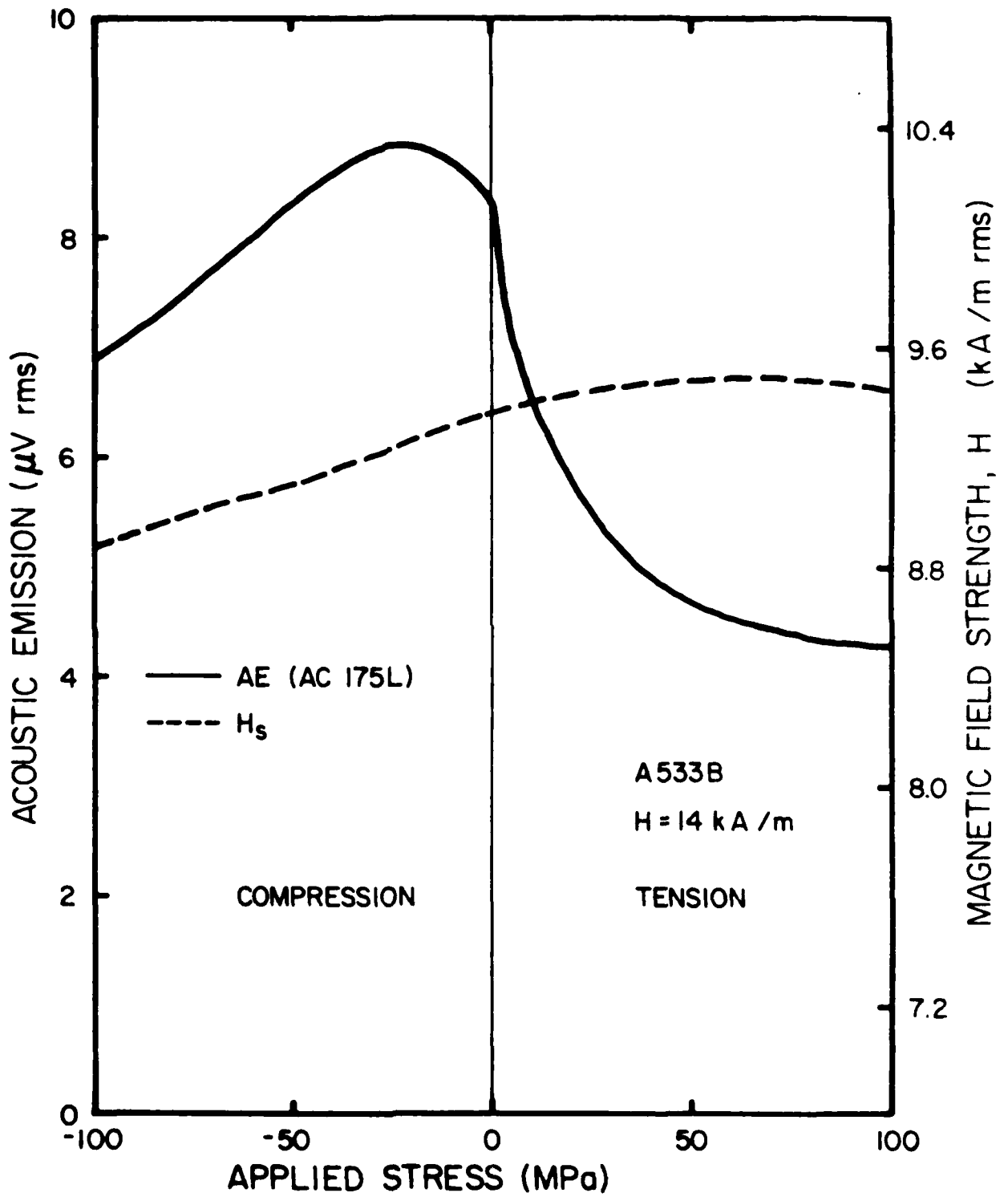


Figure 7. Acoustic emission and magnetic field strength (H_s) vs. applied stress for A533B steel at $H = 14 \text{ kA/m}$.

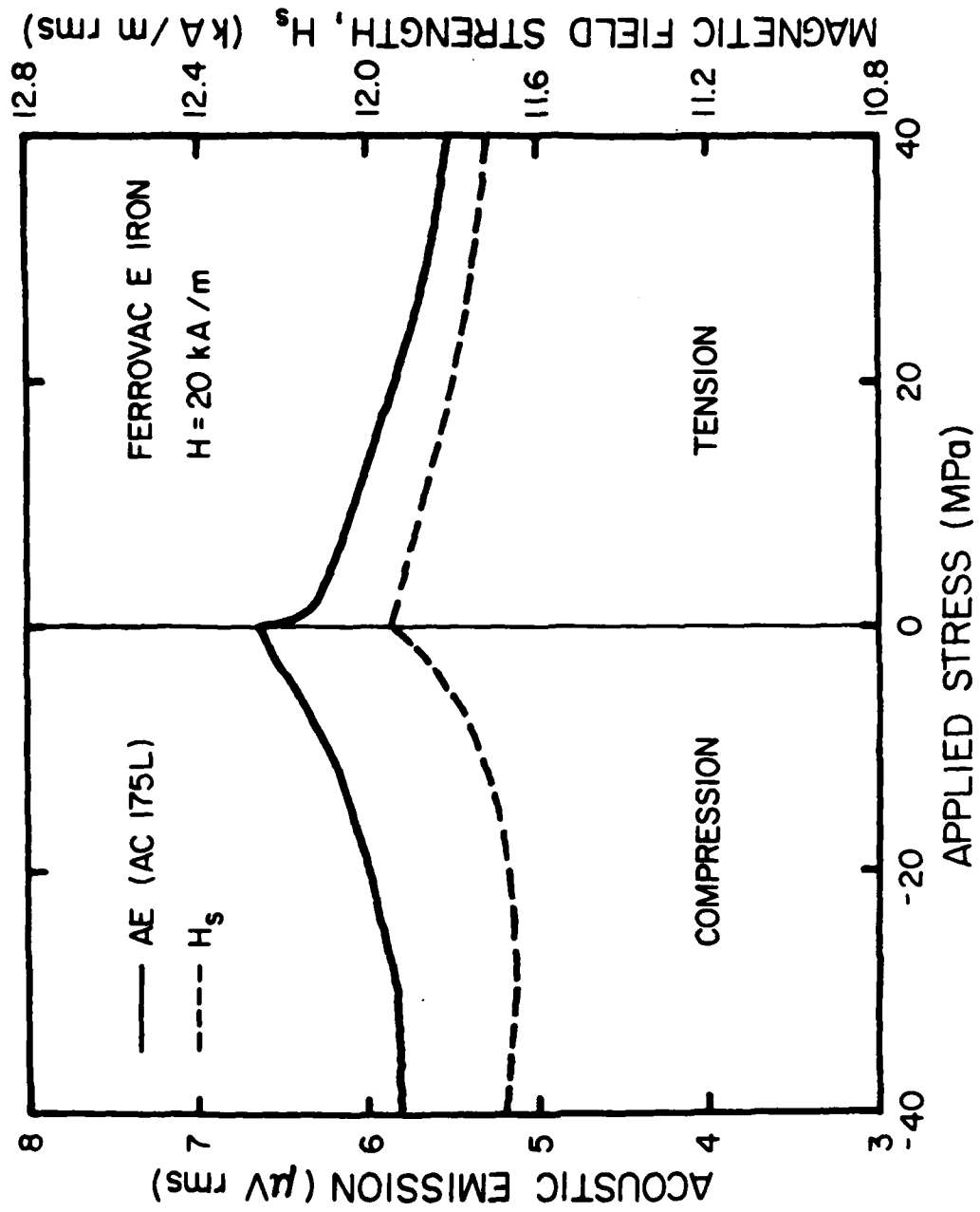


Figure 8. Acoustic emission and magnetic field strength (H_s) vs. applied stress for Ferrovac E iron at $H = 20 \text{ kA/m}$.

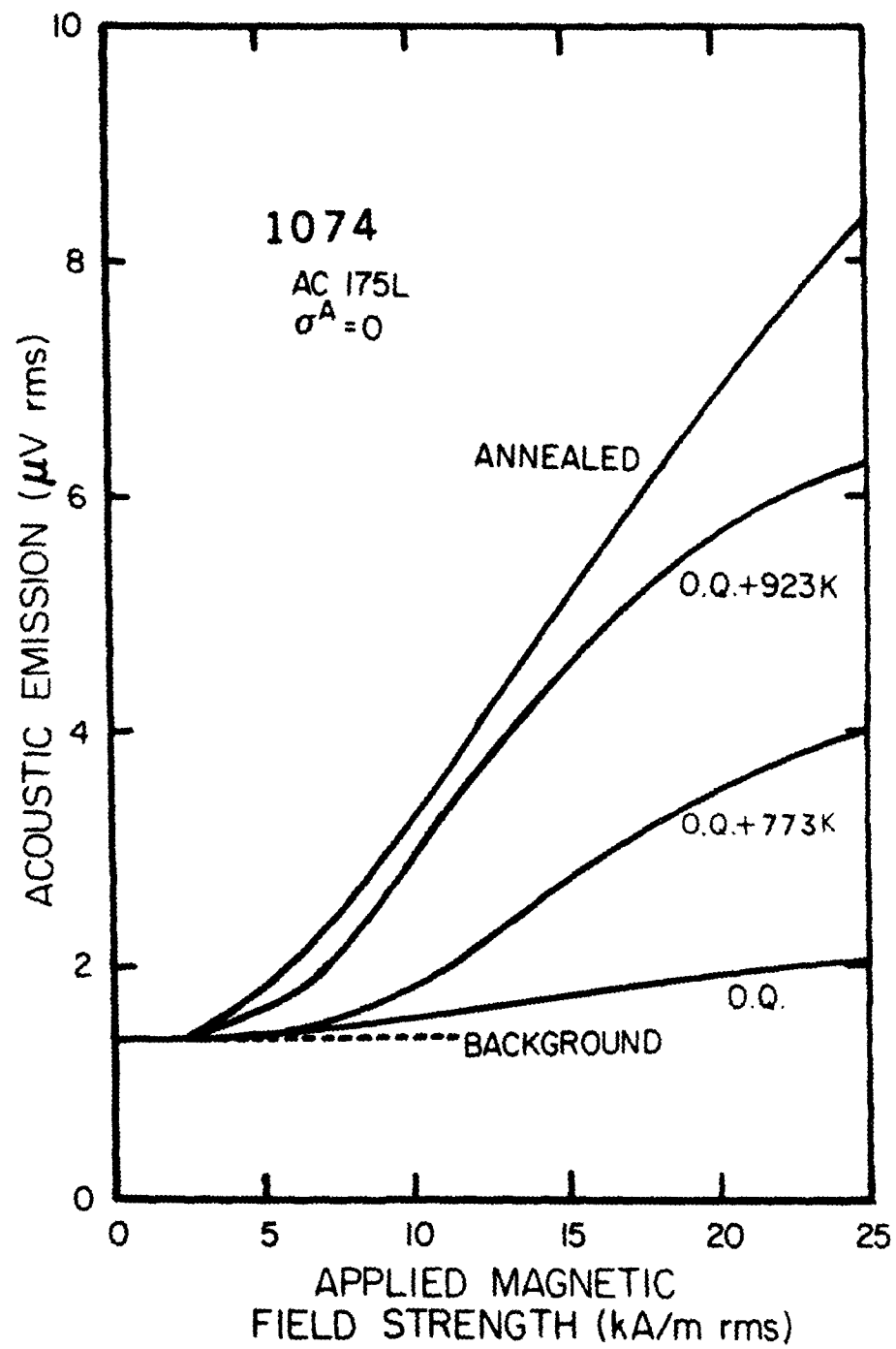


Figure 9. Acoustic emission vs. applied magnetic field strength at 175 kHz without applied stress for 1074 steel with different heat treatments.

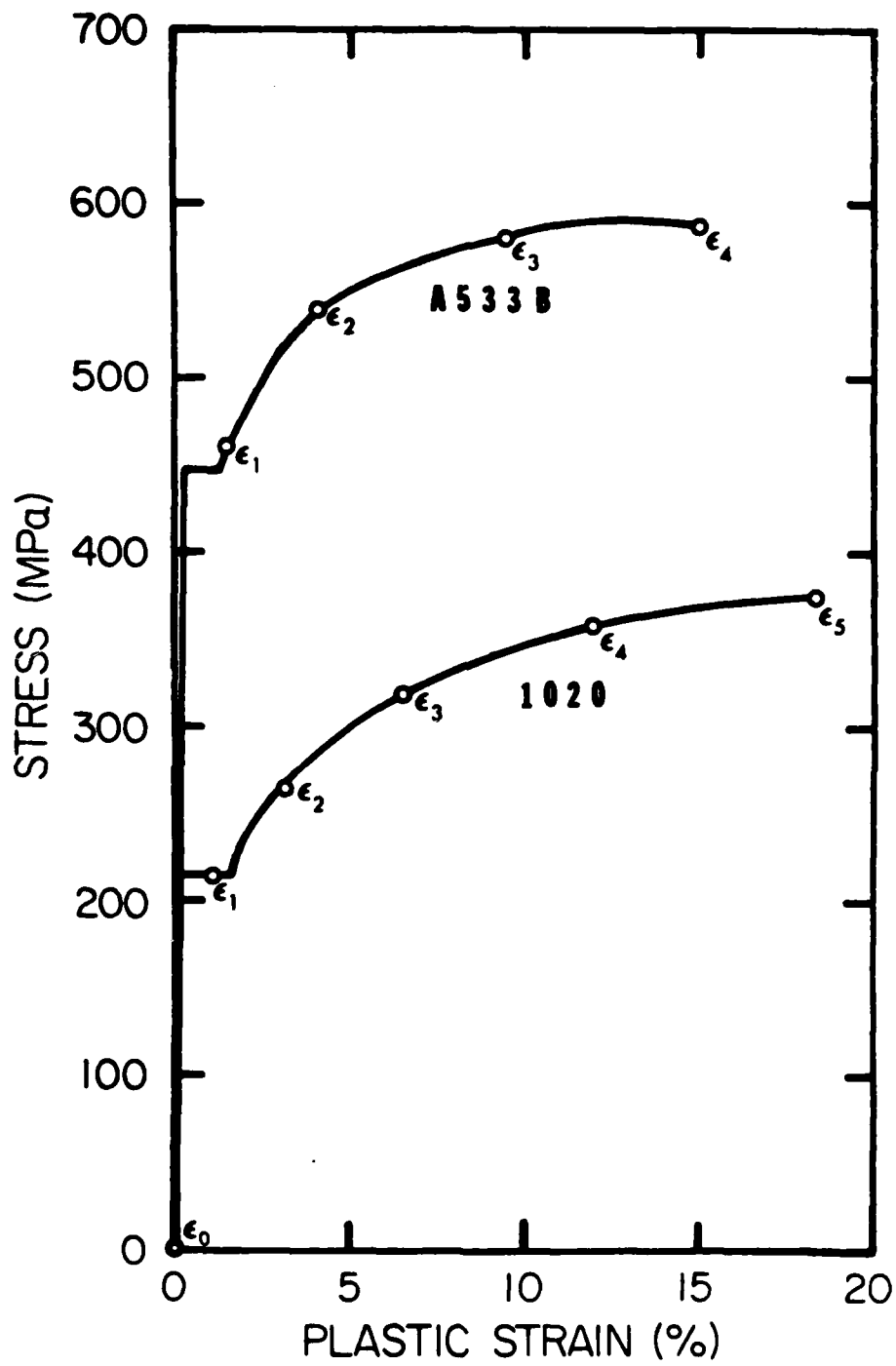


Figure 10. Stress-strain curves of 1020 and A533B steels. Circles indicate the strain levels where MAE measurements were made.

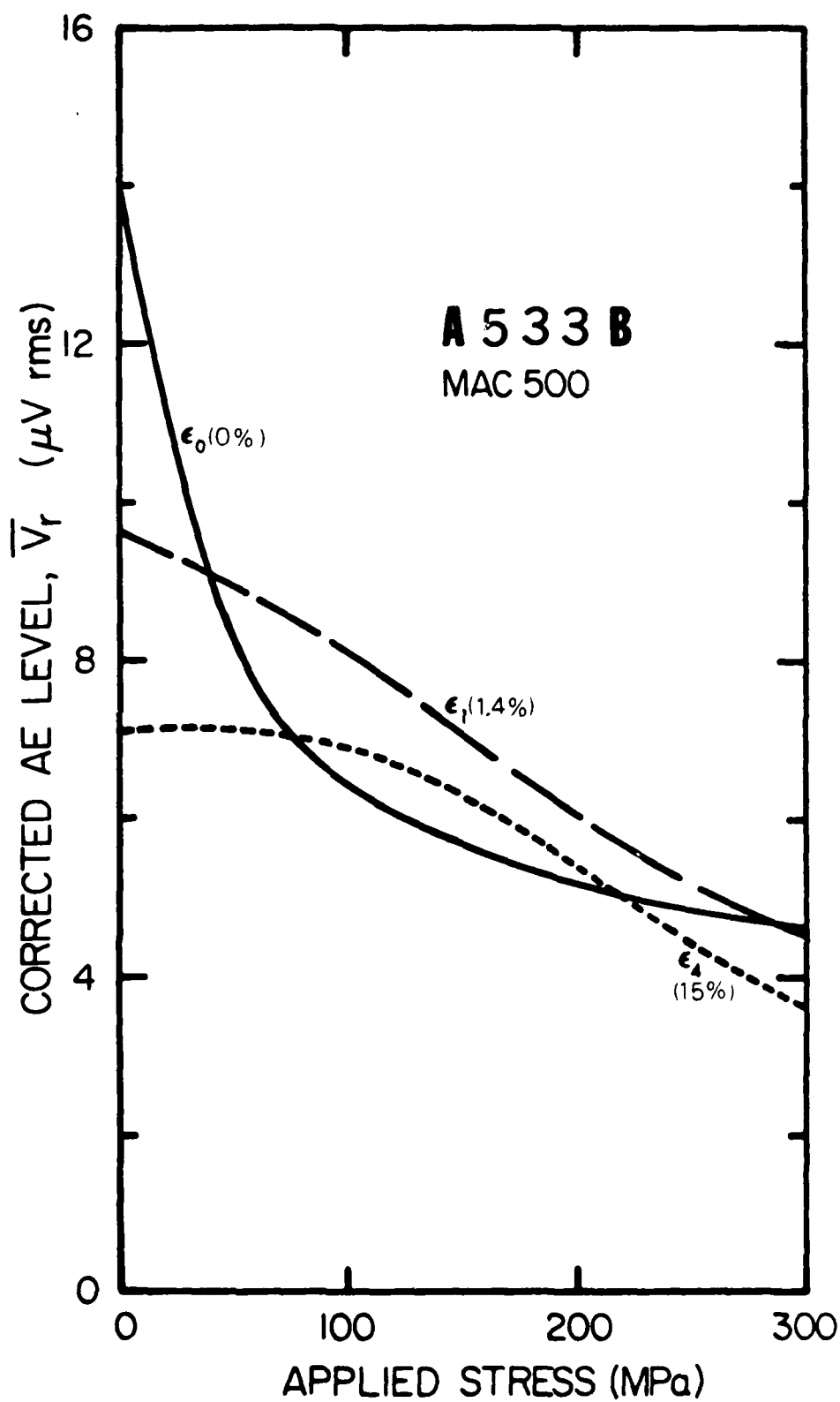


Figure 11. Background corrected AE level (500 kHz) vs. applied stress for A533B steel, deformed 0, 1.4 and 15%. Applied magnetic field strength was 22.5 kA/m.